



HAL
open science

Multi-scale transcriptome unveils spatial organisation and temporal dynamics of *Bacillus subtilis* biofilms

Yasmine Dergham, Dominique Le Coq, Pierre Nicolas, Julien Deschamps, Eugénie Huillet, Pilar Sanchez-Vizuete, Kassem Hamze, Romain Briandet

► To cite this version:

Yasmine Dergham, Dominique Le Coq, Pierre Nicolas, Julien Deschamps, Eugénie Huillet, et al.. Multi-scale transcriptome unveils spatial organisation and temporal dynamics of *Bacillus subtilis* biofilms. bioRxiv - PREPRINT, 2023, 10.1101/2023.01.06.522868 . hal-04424995v1

HAL Id: hal-04424995

<https://hal.science/hal-04424995v1>

Submitted on 29 Jan 2024 (v1), last revised 27 Feb 2024 (v2)

HAL is a multi-disciplinary open access archive for the deposit and dissemination of scientific research documents, whether they are published or not. The documents may come from teaching and research institutions in France or abroad, or from public or private research centers.

L'archive ouverte pluridisciplinaire **HAL**, est destinée au dépôt et à la diffusion de documents scientifiques de niveau recherche, publiés ou non, émanant des établissements d'enseignement et de recherche français ou étrangers, des laboratoires publics ou privés.

Multi-scale transcriptome unveils spatial organisation and temporal dynamics of *Bacillus subtilis* biofilms

Yasmine Dergham^{1, 2}, Dominique Le Coq^{1, 3}, Pierre Nicolas⁴, Julien Deschamps¹, Eugénie Huillet¹, Pilar Sanchez-Vizueté¹, Kassem Hamze^{2*}, Romain Briandet^{1*}

¹Université Paris-Saclay, INRAE, AgroParisTech, Micalis Institute, 78350 Jouy-en-Josas, France. yasmin.dorghamova-dergham@inrae.fr (Y.D.); julien.deschamps@inrae.fr (J.D.); eugenie.huillet@inrae.fr (E.H.); pilarsanviz@gmail.com (P.S.V.), *romain.briandet@inrae.fr (R.B.),

²Lebanese University, Faculty of Science, 1003 Beirut, Lebanon. *kassem.hamze@ul.edu.lb,

³Université Paris-Saclay, Centre National de la Recherche Scientifique (CNRS), INRAE, AgroParisTech, Micalis Institute, 78350 Jouy-en-Josas, France. dominique.le-coq@inrae.fr (D.L.C.),

⁴Université Paris-Saclay, INRAE, MAIAGE, 78350 Jouy-en-Josas, France. pierre.nicolas@inrae.fr (P.N.).

*corresponding authors

1 ABSTRACT

2 *Bacillus subtilis* has been extensively used to study the molecular mechanisms behind the
3 development and dispersal of surface bacterial multicellular communities. Well-structured
4 spatially organised communities (colony, pellicle, and submerged biofilm) share some
5 similarities, but also display considerable differences at the structural, chemical and biological
6 levels. To unveil the spatial transcriptional heterogeneity between the different communities,
7 we analysed by RNA-seq nine spatio-physiological populations selected from planktonic and
8 spatially organised communities. This led to a global landscape characterisation of gene
9 expression profiles uncovering genes specifically expressed in each compartmental population.
10 From this mesoscale analysis and using fluorescent transcriptional reporter fusions, 17 genes
11 were selected and their patterns of expression reported at single cell scale with time-lapse
12 confocal laser scanning microscopy (CLSM). Derived kymographs allowed to emphasise
13 spectacular mosaic gene expression patterns within a biofilm. A special emphasis on oppositely
14 regulated carbon metabolism genes (*gapA* and *gapB*) permitted to pinpoint the coexistence of
15 spatially segregated bacteria under either glycolytic or gluconeogenic regime in a same biofilm
16 population. Altogether, this study gives novel insights on the development and dispersal of *B.*
17 *subtilis* surface-associated communities.

18 **Keywords:** *Bacillus subtilis*, biofilm, swarming, transcriptome, CLSM (confocal laser
19 scanning microscopy), fluorescent transcriptional fusions, heterogeneity.

20 INTRODUCTION

21 Spatially organised communities such as biofilms exhibit a set of microbial emerging
22 properties and are embedded in a self-produced extracellular matrix^{1,2}. As these multicellular
23 communities develop, bacteria adapt and respond differently to local chemical environmental
24 conditions (*i.e.* concentration gradient of nutrient, oxygen, waste products and bacterial-
25 signalling compounds), resulting in subpopulations of cells with considerable structural,
26 physiological and biochemical heterogeneity over spatial and temporal scales³.

27 *Bacillus subtilis* has long served as a model organism for genetic studies on the formation of
28 different types of surface communities^{4,5,6,7}. This Gram-positive, motile, spore-forming
29 ubiquitous bacterium is frequently found in the rhizosphere in close proximity to plants, but
30 also in extremely various environments^{8,9}. It is commercially used to produce proteins,
31 fermented food products, biocontrol agents and probiotic^{10,11,12,13}. Conversely, it can potentially
32 play a deleterious role, like the *B. subtilis* NDmed strain, isolated from a hospital endoscope
33 washer-disinfector, capable of forming biofilms with complex protruding structures hyper-
34 resistant to the action of oxidising agents used for endoscopes disinfection, thus protecting
35 pathogenic bacteria such as *Staphylococcus aureus* in mixed-species biofilms^{14,15,16}. Hence,
36 understanding how these surface-bound communities are formed and interact is crucial for the
37 development of suitable strategies for their control.

38 In an ever-changing environment, *B. subtilis* develops different adaptation strategies to survive
39 including motility, matrix production and biofilm formation, sporulation, as well as induction
40 of other stress responses^{17,18,19}. In the laboratory, *B. subtilis* surface-associated multicellular
41 community studies are typically based on the development of a floating biofilm or pellicle at
42 the air-liquid interface, on a submerged biofilm at the solid-liquid interface, and on the
43 development of complex colony at the solid-air interface^{4,5,20}. In specific conditions, such as
44 on a semi-solid surface, *B. subtilis* cells forming the colony can become highly motile and
45 swarm over the surface by an organised collective movement while proliferating and
46 consuming nutrients²¹. On a synthetic minimal medium, *B. subtilis* swarms from the
47 multilayered colony in a branched, monolayer, dendritic pattern that continues to grow up to
48 1.5 cm from the swarm front. A transition from monolayer swarm to a multilayered biofilm
49 occurs from the base of the dendrite and spreads outwards in response to environmental
50 cues^{22,23,24,25,26}. Thus, the *B. subtilis* NDmed strain has been phenotypically well characterised

51 by multi-culturing approaches, which revealed its high ability to form 3D structures (colony,
52 submerged and pellicle) and to swarm^{4,6,27}.

53 A *B. subtilis* culture forming a biofilm contains at least seven different cell types: motile cells,
54 surfactin producers, matrix producers, protease producers, cannibal, competent and sporulating
55 cells^{1,19,28,29}. This heterogeneity, which involves differential regulation of a number of genes,
56 permits the division of labour between different cell types expressing different metabolic
57 pathways^{19,30,31,32,33,34}.

58 Temporal transcriptional analysis has been used to follow *B. subtilis* developmental strategies
59 to form a complex biofilm. A study of metabolic changes during pellicle development by
60 metabolomic, transcriptomic, and proteomic analysis, indicated that metabolic remodelling
61 was largely controlled at the transcriptional level³⁵. Besides, an ontogeny study of a *B. subtilis*
62 macrocolony growing on agar has been shown to be correlated with evolution, and a temporal
63 order of expression from older to newer genes³⁶. Recently, we have performed a transcriptional
64 study for the *B. subtilis* NDmed strain, for a whole static liquid model, in a microplate well,
65 mixed and collected on a temporal scale³⁷. This contributed to a first characterization of
66 expression profiles during the first 7 hours of submerged biofilm development and for a mixture
67 of different localised populations (submerged with detached cells and pellicle) after 24 hours
68 of incubation³⁷.

69 In the present study, we aimed to identify the differential expression of genes specifically
70 expressed in different localised compartmental populations formed on solid, semi-solid or
71 liquid interfaces. Hence, a spatial transcriptional analysis was performed at a mesoscopic scale
72 for nine different localised multicellular populations, selected from planktonic culture, static
73 liquid and swarming models. This has provided a global landscape characterization of gene
74 expression for each of the differently selected populations. Comparison between the
75 populations allowed to select 17 interesting genes whose expression was fluorescently reported
76 for real-time monitoring using 3D and 4D imaging, paying special attention to single cell scale
77 dynamics of the submerged biofilm population.

78

79

80

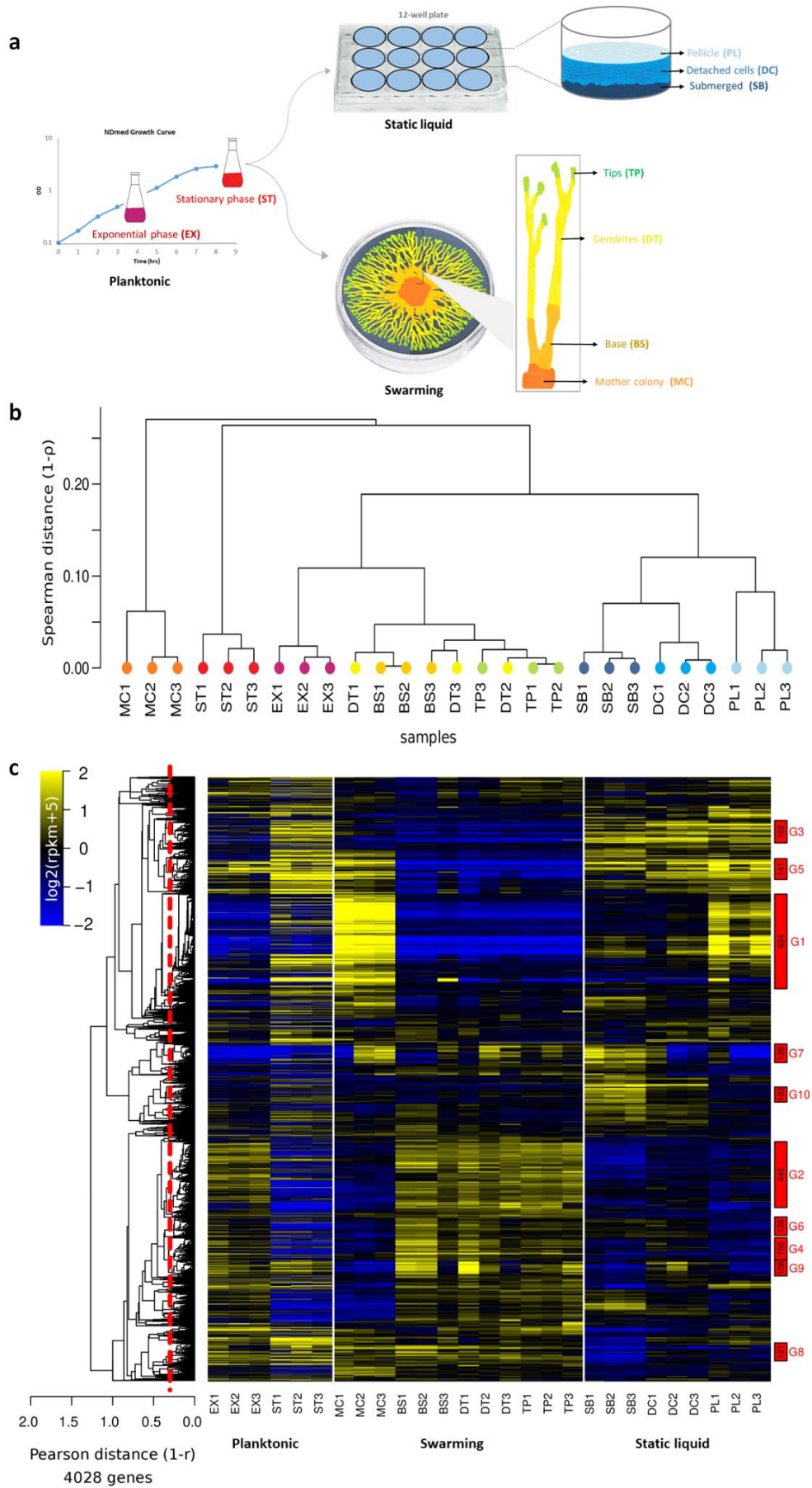
81 RESULTS

82 RNA sequencing shows spatially resolved compartmental populations with distinct 83 patterns of gene expression

84 RNA-seq was used to compare transcriptomic profiles between multicellular localised
85 populations from the different models formed by *B. subtilis* NDmed. All selected populations
86 from the different compartments are schematized in Figure 1a. We have considered a 24-hour
87 static liquid model where we have collected separately the submerged biofilm (SB), the floating
88 pellicle (PL) and the free detached cells (DC). Moreover, from a swarming model, four
89 differently localised compartments were collected; the mother colony (MC), the base of the
90 dendrites (BS), the dendrites (DT) and the tips (TP). From the planktonic culture, the
91 exponential (EX) and the stationary (ST) phases were collected, the latter being used as the
92 inoculum to initiate the two models.

93 To assess the quality and reproducibility of the RNA-seq data, a hierarchical clustering of the
94 samples was performed (Fig. 1b). This analysis shows distinct transcriptomic profiles between
95 the different spatial populations of compartments. The three biological replicates are grouped
96 together. The only exception is for the adjacent swarming compartments (BS, DT and TP),
97 where the clustering does not strictly group the samples by compartment but rather exhibits a
98 trend to separate BS-DT from DT-TP samples. This could be due to the technical difficulty to
99 precisely delineate visually these adjacent compartments, and/or because the physiology of the
100 cells in the DT could be very similar either to that in the BS or in the TP. To investigate these
101 global differences, a statistical analysis was conducted to identify differentially expressed
102 genes (DEGs) between the compartments of each model (Supplementary Fig.S1). In line with
103 the difficulty to reliably distinguish these three compartments (BS, DT, and TP), a pairwise
104 comparison for these adjacent compartments identified 12 DEGs when comparing the DT to
105 the BS and 24 DEGs when comparing the TP to the DT, with a strict increase in their number
106 to reach 304 DEGs when comparing the TP to the BS (Supplementary Fig.S1).

107



109 **Figure 1: An overview of the spatial transcriptome remodelling between the different selected compartments**
110 **of *B. subtilis*.** (a) Schematic drawing of the differently localised spatial compartments selected. From the
111 planktonic culture, the exponential (EX) and the stationary (ST) phase were selected. From the static liquid model,
112 the pellicle (PL) formed at the liquid-air interface, the submerged biofilm (SB) formed on the solid-liquid
113 interface, and the free detached cells (DC) between these two compartments were collected separately. From the
114 swarming model, four localised compartments were collected separately: the mother colony (MC), the inoculation
115 site from which the swarm has developed as a mature macrocolony; the base (BS) of the dendrites as an earlier
116 biofilm form; the dendrites (DT), a monolayer of cells ready to form later the biofilm; and the tips (TP) formed of
117 motile and highly dividing cells. For each compartment, three independent samples were taken as biological
118 replicates. (b) Pairwise distance (Spearman) between RNA-seq profiles is summarised by a hierarchical
119 clustering tree emphasising the divergence of the mother colony (MC) and the stationary phase (ST)
120 between/along other selected compartments and the closeness of the adjacent spatial compartments of either the
121 static liquid model (SB, DC and PL) or the swarming model (BS, DT and TP), which share a closer genetic
122 expression profile with the exponential phase (EX). (c) Global heatmap representation for the 4028 genes present
123 in NDmed across the spatially selected surface-associated compartments. The colour code reflects the comparison
124 to the mean computed for each gene (log₂ ratio) taking as a reference the average of all conditions, except the
125 planktonic ones (EX and ST). The hierarchical clustering tree shown on the left side of the heatmap (average link)
126 was cut at average Pearson correlation of 0.7 (dashed red line) to define the expression clusters shown as
127 rectangles on the right side of the heatmap. Clusters were named (from G1 to G321) by decreasing sizes and only
128 those containing more than 100 genes are highlighted (number of genes printed in black, cluster name printed in
129 red).

130

131 Expression profiles for the 4028 genes of *B. subtilis* NDmed along all the considered conditions
132 is presented in the heatmap Figure 1c. Groups of genes with a similar expression profile across
133 samples were identified with a cut-off on average pairwise Pearson correlation within a group
134 ($r=0.7$). The function of the genes within each of these groups of co-regulation were
135 characterised using *SubtiWiki*-derived functional categories³⁸ (Supplementary Fig.S2). The
136 largest group (G1, 634 genes), upregulated in the MC and the PL, governs around 76% of the
137 genes related to sporulation (Fig.1c, Supplementary Fig.S2). The second largest group (G2,
138 442 genes) contains 25% of the genes required for protein synthesis, modification and
139 degradation, are upregulated in the EX and in the swarming compartments (BS/DT/TP).
140 Around ~68% of the genes involved in motility and chemotaxis are clustered in G9; they are
141 downregulated in the three biofilm populations (MC, PL, and SB) and upregulated in all the
142 other compartments. Genes required for biofilm formation are mainly found in G8 with ~42%
143 of them clearly downregulated in the SB (Fig. 1c). Unknown or poorly characterised putative
144 genes constitute ~39% of the genome, among which genes with interesting profiles, *i.e.* *ywdK*,
145 *yodT*, *yjfA*, and *yezF* are highly expressed in the biofilm populations (MC, SB and PL); *yqBR*,
146 *yqzN*, *yrhG*, *ydgG* highly expressed in the TP; *ykuO*, *ywmE*, *yfmQ* highly expressed in the PL;
147 *yitJ*, *yhfS*, *yoaC*, *yaoD*, *yhfT*, *yxKC* strongly downregulated in the SB compared to other
148 compartments. To better compare the population genetic expression levels between adjacent

149 compartments and to highlight the different functional categories encoded by the differentially
150 expressed genes on a spatial level, the static liquid and the swarming models were analysed
151 separately in supplementary Fig.S3 and Fig.S4.

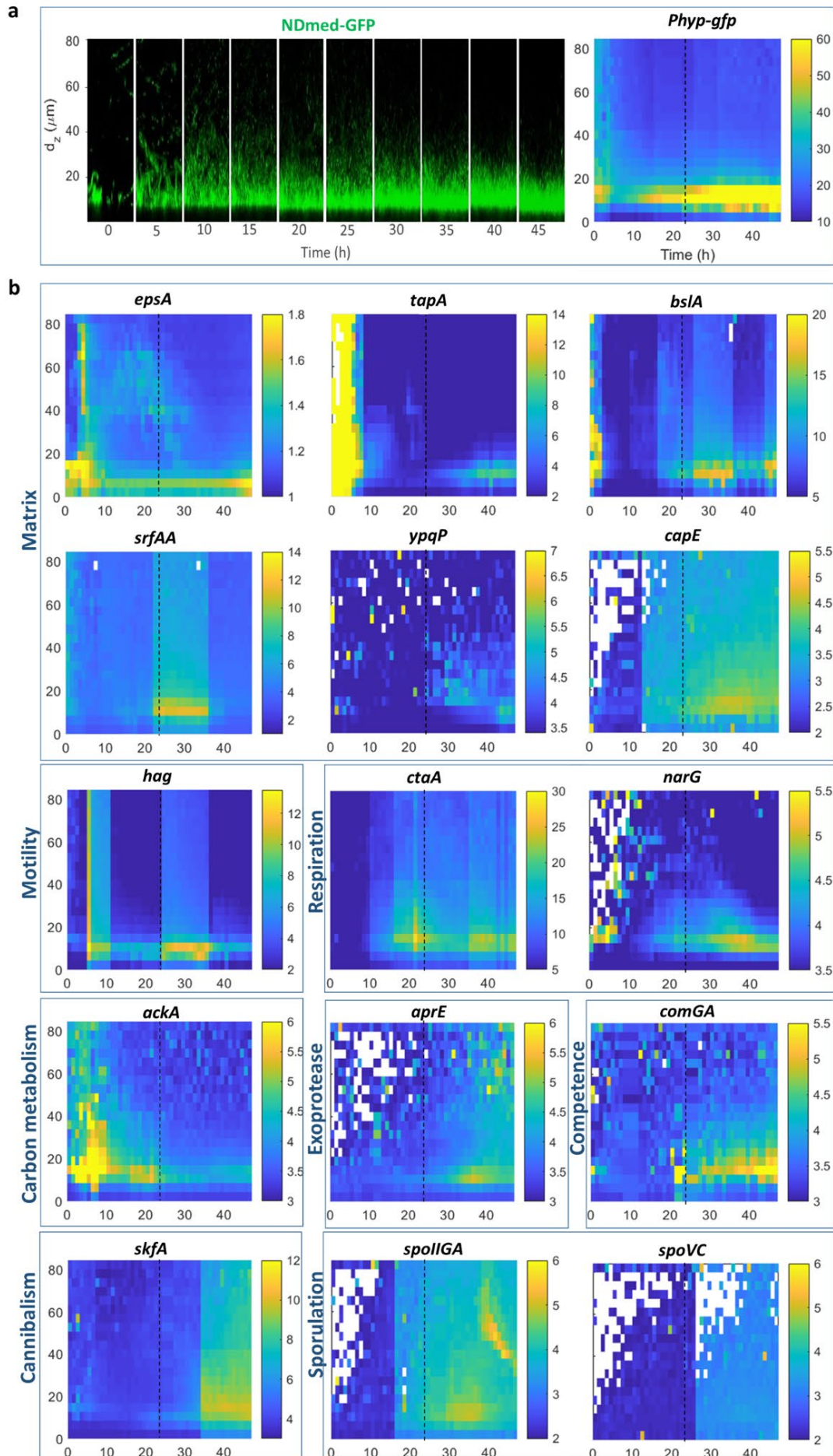
152 **Spatio-temporal patterns of gene expression reveals the various heterogeneous** 153 **subpopulations present during biofilm development**

154 Subjecting the whole compartment of a biofilm population to transcriptome analysis allowed
155 us to assess the average gene expression genome-wide but we were interested in going beyond
156 this mesoscale analysis by visualising gene expression *in situ* at a single cell level. For this
157 purpose, based on the transcriptome data and known gene functions, we identified genes
158 representing the different cell types present in a biofilm (scattered genes in the global heatmap,
159 Supplementary Fig.S5), and constructed transcriptional fusions to fluorescent reporter genes
160 *gfp* or *mCherry*. Matrix genes are represented by *epsA*, *tapA*, *bslA*, *srfAA*, *ypqP* and *capE*,
161 motility by *hag*, exoprotease by *aprE*, carbon metabolism by *ackA*, *cggR*, *gapB*, competence
162 by *comGA*, cannibalism by *skfA*, respiration by *ctaA* and *narG*, and sporulation by *spoIIIGA*
163 and *spoVC*.

164 Quantitative data from the transcriptome analysis were validated by an *in-situ* 3D microscopic
165 observation in both swarming and static liquid models, using the different reported genes
166 (Supplementary Fig.S6). Confocal imaging also pointed out spatial heterogeneity patterns of
167 gene expression along the different selected compartments. Most of the reported genes show a
168 lower or only moderately higher expression in the SB compared to the MC or the PL after 24
169 hours of incubation at 30°C (Supplementary Fig.S6). This suggests that these genes are either
170 always weakly expressed in the SB, or expressed during a short window of time before or after
171 our observation time-point (24 hours). This second hypothesis led us to monitor temporally the
172 reported genes from 0 to 48 hours of incubation.

173 A real-time movie of Gfp expression by the NDmed-GFP strain at the submerged level,
174 illustrated by a kymograph in Figure 2a, shows how cells adhere to the surface during the first
175 few hours, then stop separating out and form sessile chains, followed by a sudden
176 differentiation of a subpopulation into motile cells (between 5 and 10 hours of incubation).
177 Only in a second kinetics sessile cells colonise the surface to form the highly structured SB
178 (Supplementary Movie S1).

179



181 **Figure 2: Spatio-temporal monitoring of gene expression in submerged biofilm (SB).** (a) On the left is presented
182 4D confocal imaging (x 50 μ m, y 50 μ m, z 80 μ m) for the NDmed-GFP strain. A kymograph showing by a colour
183 code the intensity of Gfp expression as a function of time and space is presented on the right. (b) Kymographs
184 representing spatio-temporal expression of 15 transcriptional reporter fusions to genes potentially involved in
185 biofilm development. The black dotted line in each kymograph represents the time (24 hour) corresponding to the
186 RNA-seq analysis.

187 For all the reported genes, representatives of the main functional activities potentially present
188 during biofilm formation, a temporal scale monitoring the intensity of gene expression is
189 represented as kymographs in Figure 2b. Expression of *epsA* and *tapA*, involved in the synthesis
190 of the major matrix components in a biofilm, is high during the first 5 hours of SB formation,
191 followed by a global gradual decrease with some clusters remaining at high expression. Only
192 after 30 hours, a slight increase of expression is observed, homogeneously scattered on the
193 submerged level (Fig. 2b, Supplementary Movie S2). BslA, another structural protein in the
194 biofilm matrix, acts synergistically with both TasA and EPS³². In the SB, expression of *bslA* is
195 upregulated in a few clusters during the first 4 hours, followed by homogenization of a basal
196 level of expression which increases progressively with time. The *ypqP* gene, involved
197 potentially in the synthesis of polysaccharides participating in the strong spatial organisation²⁷,
198 shows some stochastic expression by very few cells at the beginning of biofilm formation; after
199 30 hours *ypqP* is expressed at a low level. In a similar manner expression of *capE*, involved in
200 capsular polyglutamate synthesis, remains at a very low level between 11 to 25 hours of
201 incubation to increase moderately afterwards. The *surfAA* gene, involved in surfactin synthesis,
202 is weakly expressed for the first 18 hours and then strongly expressed in a time frame between
203 21 and 36 hours of incubation, to be downregulated afterwards. A burst of expression of *hag*,
204 encoding flagellin, occurs after 5 hours of incubation, synchronised with the beginning of
205 down-regulation of *tapA* (Fig. 2b, Supplementary Movie S2). A gradual decrease is then
206 observed, followed by another wave of high expression of *hag* between 24 and 36 hours of
207 incubation (Fig. 2b).

208 The *ctaA* gene, encoding a heme A synthase, is one of several genes involved in aerobic
209 respiration regulated by ResD³⁹. A significant expression is observed after 8 hours of
210 incubation, followed by oscillations of high expression. Stochastic expression of anaerobic
211 genes, represented by *narG*, is observed in very few cells during the first 5 hours of incubation,
212 followed by a continuous gradual expression starting at around 14 hours.

213 For carbon metabolism, *ackA*, encoding acetate kinase, shows an upregulation during the first
214 12 hours, and is progressively downregulated after. This downregulation is faced by an

215 upregulation of *aprE*, encoding the major extracellular alkaline protease (Fig. 2b,
216 Supplementary Movie S3). A brutal expression of *comGA*, involved in competence acquisition,
217 is seen in countable cells after 21 hours giving the high expression as appearing on the
218 kymograph (Fig. 2b). This is then accompanied by an increase of the subpopulation expressing
219 moderately *comGA* (Supplementary Movie S4). Expression of *skfA*, encoding the spore killing
220 factor, is significantly observed from 21 hours with a noticeable increase in intensity after 31
221 hours of incubation (Supplementary Movie S4). We have also monitored the expression of
222 *spoIIGA* and *spoVC* involved respectively in early and late sporulation steps. Figure 2b, shows
223 that *spoIIGA* starts to be expressed at around 18 hours of incubation, indicating the beginning
224 of sporulation, while expression of *spoVC* mainly starts after around 28 hours of incubation.

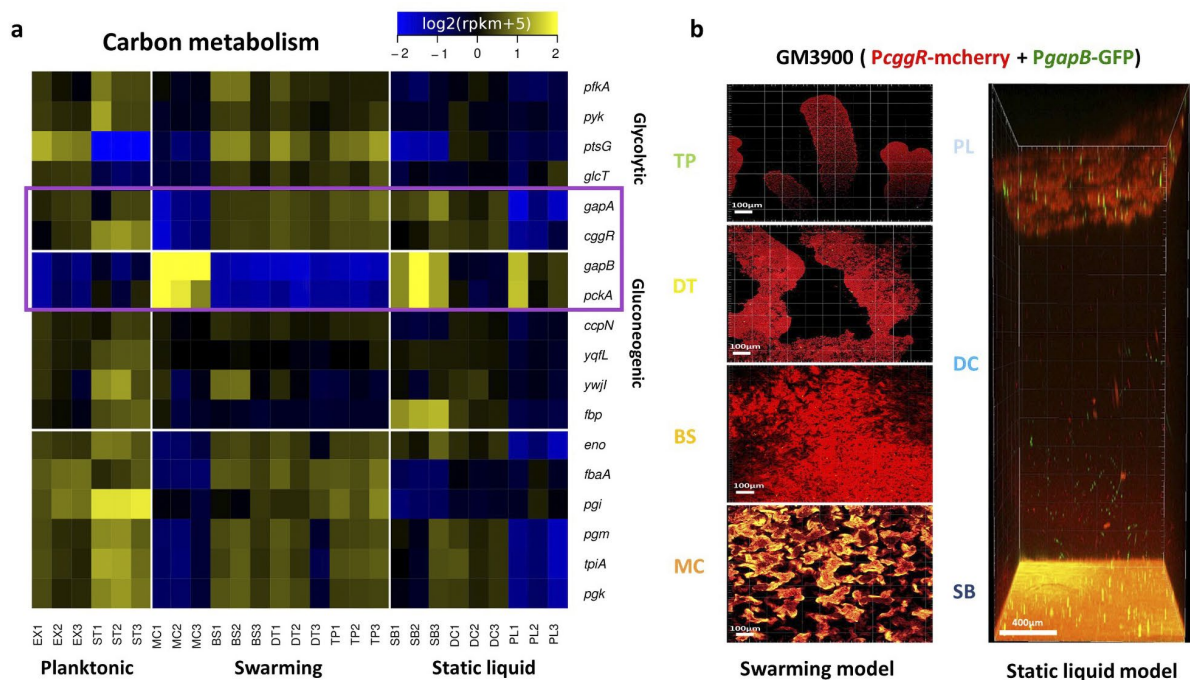
225 **Spatial transcriptome detects oppositely regulated subpopulations occurring side by side** 226 **within a biofilm**

227 Glycolysis and gluconeogenesis are two opposite pathways, for which *B. subtilis* possesses two
228 distinct glyceraldehyde-3-phosphate dehydrogenases (GAPDH) (EC 1.2.1.12) catalysing either
229 the oxidative phosphorylation of glyceraldehyde-3-phosphate into 1,3-diphosphoglycerate or
230 the reverse reaction: (i) GapA, a strictly NAD-dependent GAPDH involved in glycolysis, and
231 (ii) GapB, involved in gluconeogenesis and exhibiting a cofactor specificity for NADP⁴⁰. Since
232 coexistence of the two pathways in the same cell dissipate energy in a futile cycle⁴¹, expression
233 of *gapA* and *gapB* are subjected to very efficient opposite regulations: *gapA* transcription is
234 induced in glycolytic conditions and is repressed during gluconeogenesis by the self-regulated
235 CggR repressor of the *cggR-gapA* operon, whereas *gapB* is transcribed only during
236 gluconeogenesis and strongly repressed under glycolytic conditions by the CcpN repressor, as
237 is *pckA*, encoding the purely gluconeogenic PEP-carboxykinase (PEP-CK)^{40,42,43}.

238 Although cultures for this study were performed in purely glycolytic conditions (*i.e.* with
239 glucose as a carbon source), we have observed (Fig. 3a) that in the three biofilm populations
240 (MC, SB, and PL) expression of *gapB* and *pckA* was derepressed after 24 hours of incubation,
241 indicating a depletion in glucose in these compartments. Interestingly, the two strictly
242 oppositely regulated groups of genes, *cggR-gapA* on one hand, or *gapB* and *pckA* on the other
243 hand, are oppositely regulated in all the different selected compartments, except in the SB
244 where these 2 groups are both upregulated (Fig. 3a). This observation suggested coexistence
245 of two cell types in the same compartment and motivated the construction of a strain reporting

246 the expression of both *cggR-gapA* and *gapB* by different fluorescent transcriptional fusions
 247 (Table 1).

248 Using this strain (GM3900) and CLSM imaging, we observed at a single cell level the *in-situ*
 249 expression of both GapA and GapB in the different spatially localised populations of
 250 compartments. Figure 3b represents a real-time spatial monitoring after 24h for the different
 251 compartments of a swarming model (MC, BS, DT, and TP) and a static liquid model (PL, DC,
 252 and SB). Observation of GM3900 swarming on a glycolytic medium clearly confirmed our
 253 previous transcriptome data, from which the glycolytic genes *gapA* and *cggR* appeared
 254 upregulated all along the swarming compartments (BS, DT, and TP) and were rather
 255 downregulated in the MC. On the contrary, the gluconeogenic genes *gapB* and *pckA* were
 256 repressed in the swarming compartments, and highly upregulated in the MC. In the static liquid
 257 model, gluconeogenic genes were upregulated in both the PL and the SB compartments; an
 258 upregulation of glycolytic genes was also observed in both the SB and the DC compartments.
 259 Microscopy observations allowed to display the coexistence of subpopulations under either a
 260 glycolytic or a gluconeogenic metabolic regime in all the three biofilm compartmental
 261 populations (PL, SB and MC).



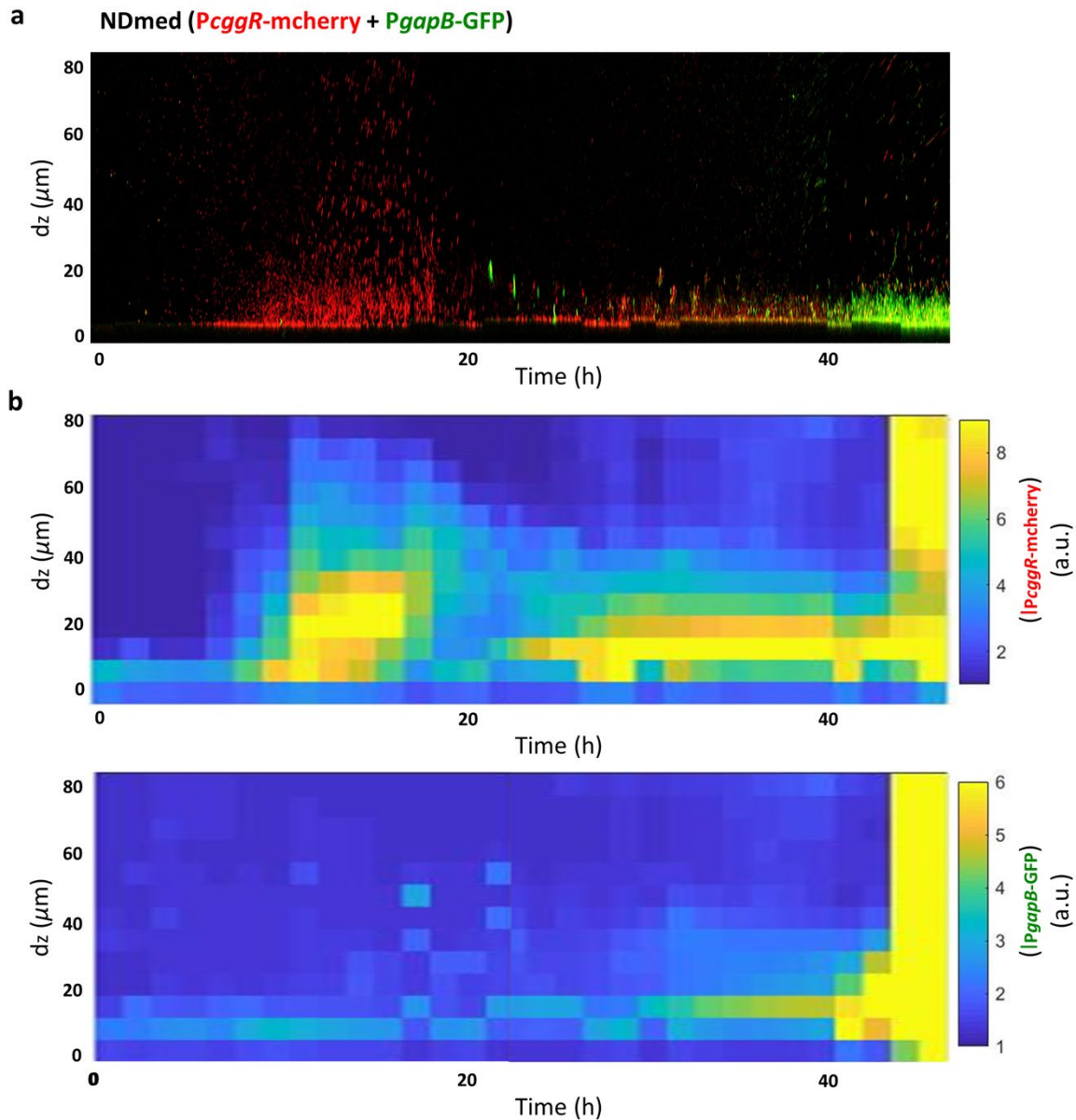
262

263 **Figure 3: Spatial transcriptomic remodelling with in situ 3D imaging highlights a heterogeneous differential**
 264 **expression of central carbon metabolism.** (a) Heatmap representation of the relative variations of expression
 265 level across samples. The colour code reflects the comparison to the mean computed for each gene across all the

266 *samples, except the planktonic (EX and ST) (log₂ ratio). Genes were selected from Subtiwiki categories specific*
267 *for glycolysis or gluconeogenesis, or common to both pathways (level 3). The purple box highlights central genes*
268 *specific respectively for glycolysis (gapA, cggR) or gluconeogenesis (gapB, pckA). (b) Spatial confocal imaging*
269 *for the different selected compartments from the swarming (MC, BS, DT, TP) and the static liquid (SB, DC, TP)*
270 *models after 24 hours at 30°C. Using strain GM3900 reporting transcription of cggR-gapA by mCherry (in red)*
271 *and of gapB by gfp (in green), with the same protocol as for the transcriptome analysis, except for the static liquid*
272 *model the usage of 96-well microplate instead of the 12-well. Three replicative observations were performed*
273 *independently for each model.*

274 **Conversion from glycolytic to gluconeogenic regime starts from localised single cell** 275 **within a glycolytic expressing population**

276 Most of the physiological and genetic studies on regulation of carbon central metabolism and
277 glycolysis/gluconeogenesis have been performed with planktonic liquid cultures in defined
278 media, laboratory conditions not reflecting the complexity of the regulations involved in
279 bacterial natural habitats. A closer observation to the BS, in the swarming model, or to the PL,
280 in the static liquid model, allowed to visualise in GM3900 the switch to a gluconeogenic regime
281 occurring in a single cell from a population growing with a glycolytic metabolism (Fig. 3,
282 Supplementary Fig.S7). We then performed *in situ* spatio-temporal scale monitoring for the
283 submerged compartment with a higher resolution (Fig. 4). 4D confocal imaging of GM3900
284 shows a high expression of glycolytic genes in bacteria growing in the glycolytic B medium
285 (Supplementary Movie S5). After 15 hours of incubation, as nutrients become limited, there is
286 a gradual decrease of cells expressing glycolytic genes, followed by a sudden expression of
287 gluconeogenic genes in small clusters of few cells. Cells under a glycolytic regime continue to
288 decrease with an upregulation of gluconeogenesis in a few other cells. Then after 22 hours cells
289 regain a glycolytic metabolism and after 24 hours most of the population is again in glycolysis,
290 but with some clusters of cells in gluconeogenesis (Fig. 4). After 24 hours, one can observe a
291 slight increase in the number of cells of both subpopulations expressing either glycolytic or
292 gluconeogenic genes being spatially mixed together, followed after 42 hours by strict increase
293 in subpopulations expressing opposite carbon metabolism regulatory pathways
294 (Supplementary Movie S5). Even after prolonged incubation these subpopulations seem to
295 remain associated together. These observations indicating the coexistence of spatially mixed
296 subpopulations growing either under a glycolytic or gluconeogenic regime in all the three
297 biofilm populations (MC, PL and SB) suggest the existence of metabolite exchange between
298 these subpopulations. Besides, another source of metabolites could be provided by dead cells.



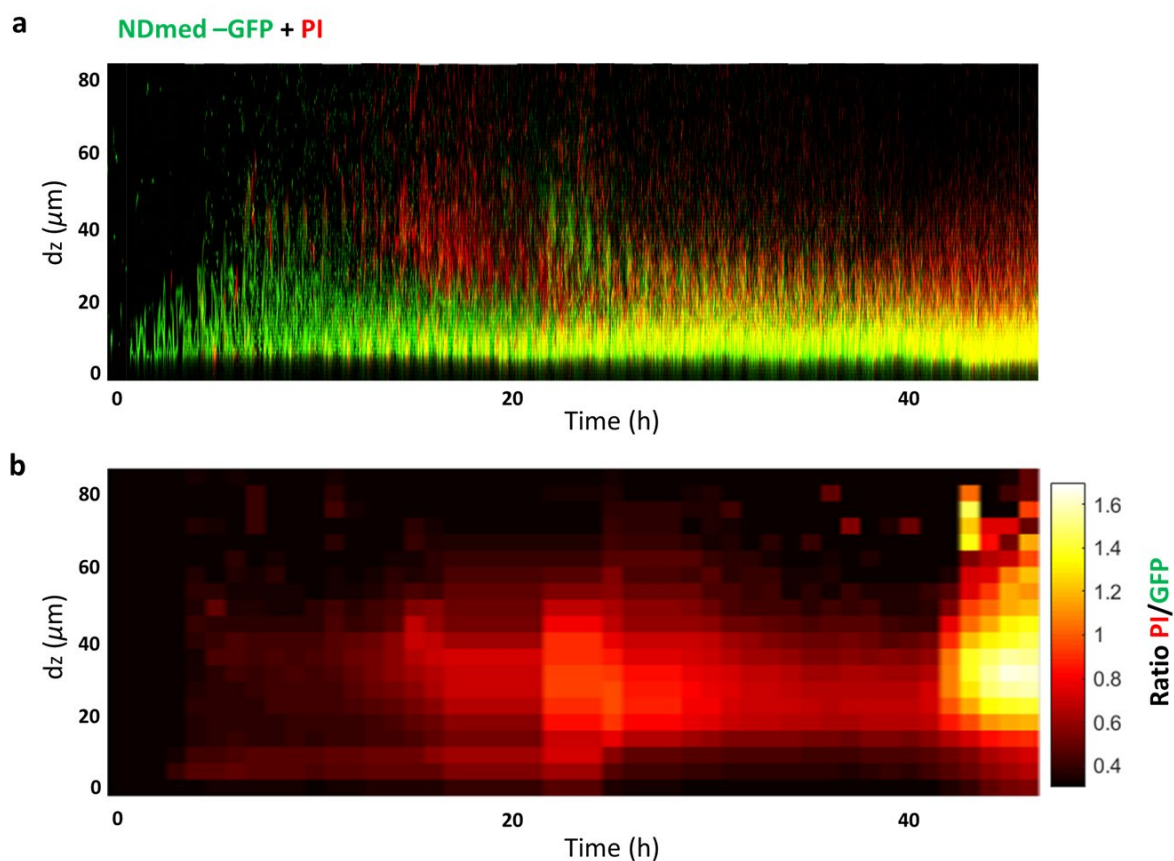
299

300 **Figure 4: Spatio-temporal imaging for the submerged biofilm compartment.** (a) Sections from a real-time
301 confocal imaging ($x\ 50\mu\text{m}$, $y\ 50\mu\text{m}$, $z\ 80\mu\text{m}$) for 48 hours, image every one and half hour, using strain GM3900
302 reporting transcription of *cggR* (*gapA*) by *mCherry* (in red) and of *gapB* by *gfp* (in green), with the same protocol
303 used for the transcriptome analysis, except the usage of 96-well microplates instead of the 12-well (Supplementary
304 Movie S5). (b) Kymographs representing by a colour code the intensity of the expression for the transcriptional
305 reporter fusions to the *cggR* and *gapB* genes along a spatio-temporal scale. Three biological replicates were
306 performed.

307 Two successive waves of localised cell death remodel the biofilm organisation

308 To further understand the heterogeneity and fluctuations of the different functions during *B.*
309 *subtilis* biofilm development, a Live/Dead tracking at single cell scale was performed. Figure

310 5a, represents kinetic images for the live cells of *B. subtilis* reported by their expression of
311 green fluorescent protein (GFP, green), while the dead cells and eDNA were contrasted with
312 propidium iodide staining (PI, red). A multidimensional kymograph representing the intensity
313 of dead cells (obtained by a ratio of dead/live cells) as a function of their spatial localization
314 and time is presented in Figure 5b. Bacteria adhere to the surface and form chains of sessile
315 cells in the first few hours of incubation and thereafter, between 15 and 24 hours, clusters of
316 dead cells are observed over the formed biofilm (Fig. 5, Supplementary movie S1). After this
317 first wave, the dead cells density decreases (Fig. 5), faced by a slight increase in the live
318 population until around 42 hours where a second wave of dead cells occurs (Fig. 5a,
319 Supplementary movie S1). Interestingly, by comparing the kymographs in Figures 2a and 5b,
320 it appears that these dead cells subpopulations are mainly spatially localised as a layer on the
321 top of the SB live cells.



322

323 **Figure 5: Temporal observation for the submerged biofilm (SB) development reveals oscillations of dead cell**
324 **spatial localization.** (a) Sections from a real-time confocal imaging (x $50\mu\text{m}$, y $20\mu\text{m}$, z $80\mu\text{m}$), image every one
325 hour, using NDmed-GFP (GM3649) and PI for permeable cell staining, with the same protocol used for the
326 transcriptome analysis, except the usage of 96-well microplates instead of the 12-well (Supplementary Movie S1).
327 (b) Kymograph representative of at least three replicates, representing the ratio of dead/live cells along a spatio-
328 temporal scale.

329 DISCUSSION

330 Spatial transcriptomic data generated in this study put forward a global view on the variation
331 of gene expression profiles for nine localised compartments, including three biofilm
332 populations: the MC, PL and SB. A global hierarchical clustering of the RNAseq analysis (Fig.
333 1b) points out that the MC formed on agar showed a very distinct transcriptome profile
334 compared to the PL and the SB. With the different environmental conditions, similarities could
335 still be exhibited between the different biofilm populations. For instance, the *hag* gene
336 encoding flagellin and reporting motility is downregulated in the three biofilms compared to
337 the other compartments explored (DC, BS, DT, and TP). Microscopy observations of
338 fluorescent transcriptional fusion further allowed to contrast minor subpopulations of cell
339 expressing motility genes, in particular on the interfacial layers of the community, *i.e.*
340 embedded under matrix-producing cells. This corresponds to the layer near to the agar surface
341 for the MC; the inner immersed layer for the floating PL, and the layer in contact with the
342 substratum for the SB (Supplementary Fig.S6). Expression of flagella could also be present
343 within the biofilm indicating the migration of cells by chemotaxis toward a zone richer in
344 oxygen and nutrients, allowing the vascularization of the biofilm matrix to increase
345 diffusion/reaction throughout the biofilm⁴⁴.

346 Most of the genes involved in sporulation appear strongly upregulated in aerial biofilms (MC
347 and PL) and poorly expressed in the SB community. Surprisingly, in the static liquid model, a
348 specific counting of spores indicated a higher quantity in the SB fraction than in the PL (data
349 not shown), although sporulation genes were more expressed in the PL. Indeed, it has been
350 shown recently that the spore surface of *B. subtilis* was covered with legionaminic acid,
351 required for the crust assembly and enhancing hydrophilicity⁴⁵. All together these observations
352 suggest that, in the timeframe we explored, spores essentially produced in the PL can sediment
353 as hydrophilic colloids down the well and accumulate within the SB level. Another striking
354 difference between these compartments is the dominant anaerobic respiration metabolism
355 detected in the SB compared to the other aerial biofilm populations. Within a static liquid
356 model, the coexistence of two interfacial biofilm communities of *B. subtilis* with distinct
357 respiration metabolisms is pointed out here: the SB (and the DC) mainly under anaerobic, and
358 the PL under aerobic respiration. Although the PL and the MC are in contact with the air, the
359 existence of a small subpopulation of cells expressing anaerobic genes is still observed. Taking
360 advantage of RNA-seq data and of transcriptional reporter fusions associated with the

361 microscopy technique, we could observe that the major extracellular matrix genes (*i.e. epsA-*
362 *O, tapA* operons, and *bslA*) are more strongly and homogeneously expressed in the aerial
363 biofilms than in the SB, which forms small dispersed clusters. This diversity in the spatial
364 repartition of cells producing each of these matrix components suggests different biochemical
365 matrix composition associated with specific local micro-rheological properties. For better
366 visualisation of the genetic expression level among adjacent compartments, the swarming
367 model and the static liquid model were analysed separately (Supplementary Fig.S3 and Fig.S4).

368 Transcriptome analysis of four different spatial compartments of the swarming model allowed
369 to highlight the sequential gene regulations taking place during bacterial surface colonisation.
370 A huge divergence in gene expression is observed between the MC and the three other
371 compartments, including its adjacent compartment BS. These compartments govern
372 metabolically active cells displaying a high upregulation of genes involved in several functions,
373 essentially related to active growth: replication and division (*dnaAN* and *ftsEX* operons,
374 *divIVA*), transcription and translation (*rpoA*, *pur* and *pyr* operons, *tRNA*, *rRNA*, ribosomal
375 proteins genes), energy metabolism (glycolytic genes, thiamin and biotin biosynthesis),
376 transport (several genes encoding transporters of various carbon and nitrogen sources such as
377 amino acids, or transporters of different metal ions), motility and chemotaxis (*fla/che* operon,
378 *hag*, *ycaA*). On the other flip, genes related to sporulation and gluconeogenic carbon
379 metabolism are more expressed in the MC compared to the BS, DT and TP compartments,
380 indicating that stress signals such as nutrient depletion initiated the sporulation process to face
381 the harsh environmental conditions. Matrix related genes are more upregulated in the MC and
382 the BS compared to the DT and TP, which is clearly observed by confocal imaging of the
383 distribution of these subpopulations during a swarm (Supplementary Fig.S6). The regulations
384 of these latter genes indicate that cells in the TP are more exploring the environment to
385 incorporate nutrients from the medium, rather than expressing proteins involved in biofilm
386 formation or sporulation, contrary to cells in the BS. Thus, each compartment is formed by
387 cells under different physiological states with higher cellular heterogeneity going toward the
388 MC.

389 Between adjacent static liquid compartments, half of the genome is differentially expressed
390 with two biofilm populations coexisting in the same well. The DC (compartment between the
391 two biofilms) have been long considered as a state similar to the planktonic population.
392 Phenotypic and transcriptomic studies on various bacterial species, such as *Klebsiella*

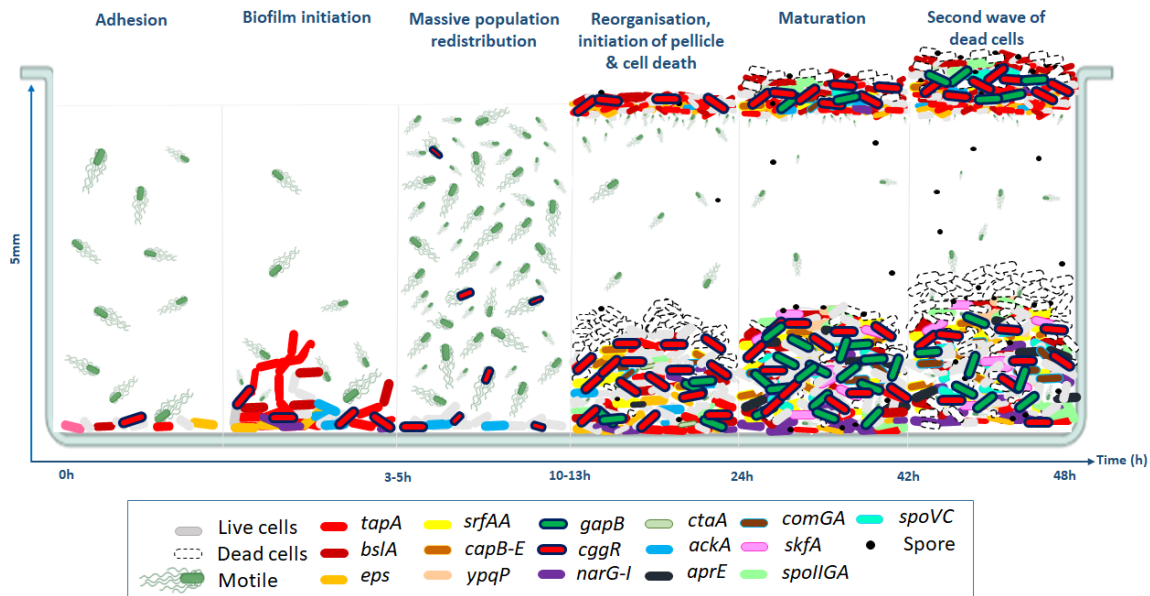
393 *pneumoniae* or *Streptococcus pneumoniae*, have shown that detached cells exhibit different
394 gene expression patterns, distinct from both sessile and planktonic lifestyles^{46,47,48,49}. Our
395 results with *B. subtilis* confirm these previous observations. The transcriptome profile of the
396 DC revealed a distinct state compared to both EX and ST planktonic phases as well as to the
397 two biofilms in the static liquid model. For instance, the major matrix genes of the *tapA* and
398 *epsA-O* operons, are downregulated in the DC compared to both the ST and the EX phases.
399 These operons are more expressed in the DC and the PL than in the SB.

400 A spatio-temporal monitoring on the submerged level, revealed patterns of gene expression
401 linked to the phenotypic heterogeneity observed during the different stages of biofilm
402 development. We could highlight the heterogeneous expression of the different matrix genes
403 (*epsA-O*, *tapA*, *bslA*, *srfAA*, *ypqP*, and *capB-E*) over both spatial and temporal levels. EPS and
404 TasA are highly produced in the first few hours of incubation during the adhesion and
405 development of the biofilm to the surface. The latter matrix components are assembled by
406 BslA, required for biofilm architecture and biofilm hydrophobicity of the colony and
407 pellicle^{32,50}. In a previous study, we reported that *bslA* inactivation had an impact on the 3D
408 structure of the colony and also on the stability of the pellicle, while no effect was observed for
409 the submerged biofilm compartment after 24 hours of incubation⁶. 4D-CLSM allowed to
410 demonstrate that *bslA* is expressed during the first 3 hours of SB development (together with
411 the *epsA-O* and *tapA* operons) and then again in late stage of biofilm maturation after 17 hours,
412 when the biofilm is already formed. A strong correlation between biofilm development and
413 surfactin production was suggested within different *Bacillus* species. For instance, in *B.*
414 *velezensis* FZB42, *B. amyloliquefaciens* UMAF6614 and *B. subtilis* 6051 defect in surfactin
415 production has been shown to cause partial or severe biofilm defects^{51,52,9}. On the other hand,
416 in the *B. subtilis* strains NCIB3610 and NDmed, surfactin operon mutation was reported not to
417 have any effect on biofilm formation (pellicle, colony and submerged)^{6,53}. As an external
418 signal, surfactin induces cells to express matrix genes¹. The *srfAA* gene is expressed mainly in
419 a temporal window between 21 and 36 hours during biofilm incubation after which one can re-
420 observe expression of the EPS and TasA. In addition, the late expression of *ypqP* and *capE*
421 observed in our imaging data is consistent with the small effect on biofilm formation at 24
422 hours previously reported for inactivation of these genes⁶. Only a subpopulation of the SB
423 expresses the different matrix genes. Hence, heterogeneous spatio-temporal expression of
424 matrix genes indicates specific requirements of the expensive matrix products through the
425 different stages of biofilm development.

426 In a medium containing carbon and nitrogen excess, a major overflow pathway takes place
427 through the conversion of pyruvate to acetate by the phosphotransacetylase-acetate kinase
428 pathway to generate ATP. This pathway is positively regulated by a major regulator for the
429 carbon metabolism CcpA which for instance activates the *ackA* gene, encoding an acetate
430 kinase⁵⁴. In this study we could see that *ackA* and the *cggR-gapA* operon (reporting glycolysis)
431 were highly expressed during the first 13 hours, before being gradually downregulated,
432 indicating that carbon source started to be limited afterwards (Fig. 2 and Fig. 4). Interestingly,
433 this corresponded with the beginning of the first wave of dead cells that was clearly observed
434 after 13 hours (Fig. 5), followed by the initiation of sporulation reported by *spoIIGA* (Fig. 2).
435 Hence, these observations suggest that carbon source limitation triggered cell death which by
436 turn provided carbon source for the initiation of the irreversible sporulation process. Cell death
437 is also followed by competent and cannibal cell types, tagged by *comGA* and *skfA* genes,
438 overexpressed at around 20 hours (Fig. 2), pointing out the capability of these cells to uptake
439 exogenous DNA from the medium and produce spore-killing factors, allowing to delay their
440 entry into the irreversible process of sporulation¹⁹. After the first wave of dead cells a slight
441 increase in the live population was observed (Fig. 5, Supplementary Movie S1), which
442 accommodates different subpopulations expressing either glycolysis or gluconeogenesis.
443 Another expression of the *hag* motility gene is observed after 24 hours in a small subpopulation
444 of the SB. This could correspond to pore forming swimmer cells as previously observed⁴⁴.
445 Surfactin, reported by *srfAA*, is overproduced around the same spatio-temporal window.
446 Surfactin is involved in genetic competence and triggers matrix production^{5,31,55,56}, in
447 accordance with the upregulation of the genes *epsA-O*, *tapA*, *bslA*, *ypqP*, *capB-E* and *comGA*
448 after 24 hours of incubation. Motility could also allow to increase the diffusion and activity of
449 exoproteases (product of the *aprE* gene, among others) within the matrix biofilm. Moreover,
450 cells undergoing sporulation are also present at that time as indicated by the overexpression of
451 late sporulation genes (such as *spoVC*).

452 A highly structured colony has wrinkles, formed by mechanical forces due to increased cell
453 density. Dead cells localised under these wrinkles, at the base of the biofilm and near the agar,
454 lead to formation of channels that facilitate liquid transport within the biofilm^{57,58}. In the SB,
455 *B. subtilis* dead cells are clustered mainly on the top of the biofilm appearing in two waves
456 during 13-24 hours and after 42 hours. The second wave of dead cells (after 42 hours) is also
457 in the same accordance with the high expression of gluconeogenic genes (reported by *PgapB-*
458 *gfpmut3*, Fig. 4). Despite that the DC at 24 hours are distinct from the planktonic populations

459 (EX and ST) but are still in a physiological state closer to cells in EX rather than ST ones (Fig.
 460 1b). This is illustrated by the extremely strong upregulation (around $9\log_2FC$) of the *pstS-BB*
 461 and *tuaA-H* operons in the ST compared to the DC or the EX. These operons, involved in high-
 462 affinity phosphate uptake and teichuronic acid biosynthesis, respectively, are induced upon
 463 phosphate starvation⁵⁹, which indicates that DC, like cells in the EX, do not suffer such
 464 conditions, contrary to cells in ST.



465

466 **Figure 6: Spatio-temporal diversification of *B. subtilis* cell types in a well of microplate.** A schematic illustration
 467 proposed for the static liquid biofilm dynamics over 48 hours, using a microplate and different reporting
 468 techniques. First, cells adhere to the submerged surface, followed by biofilm initiation where adherent sessile
 469 cells proliferate expressing matrix genes (i.e. *tapA* and *eps*). This is followed by a massive population
 470 redistribution, during which a sudden cell differentiation from sessile to motile cells occurs within a 15 minutes
 471 range. Then the submerged biofilm is reorganised and the formation of a pellicle is initiated at the air-liquid
 472 interface. This is accompanied by a 1st localised cell death wave (between 13 and 24 hours). Maturation of biofilm,
 473 associated with a slight increase in the live population is followed by a 2nd wave of cell death (after around 42
 474 hours).

475 This report presents the first comparative description of the transcriptomic profiles of nine
 476 spatio-physiological populations of *B. subtilis* captured on solid, semi-solid and liquid cultures
 477 using the same strain and nutrient source. It allowed us to specify the singularities of each
 478 biofilm compartment and to pinpoint the fineness of their spatio-temporal regulation down to
 479 the single scale. The presented data give novel insights on the development and dispersal of *B.*
 480 *subtilis* surface-associated communities, with a special comprehension for the relation between
 481 central carbon metabolism regulation and dead cells on the submerged level (Fig.6). All the

482 provided results summarised could serve as a unique resource for future studies on biofilm
483 physiology to further investigate genetic determinants required for its control.

484

485 METHODS

486 *Bacterial strains and growth conditions*

487 The *B. subtilis* strains used during this study are listed in Table 1. NDmed derivatives were
488 obtained by transformation with various plasmids or chromosomal DNA of various strains to
489 introduce the corresponding suitable reporter fusion. The transcriptional fusions of the *gfpmut3*
490 gene to the *ackA*, *hag*, *bslA*, *srfAA* or *gapB* promoter were constructed previously within the
491 pBSB2 plasmid (pBaSysBioII) using ligation-independent cloning⁶⁰, prior to integration into
492 the chromosome of BSB168 in a non-mutagenic manner, resulting in strains BBA0093,
493 BBA0231, BBA0290, BBA0428 and BBA9006, respectively; chromosomal DNA of each
494 strain was used to transfer the corresponding fusion into NDmed by transformation. Similarly,
495 fragments corresponding to the promoter regions of *epsA*, *ypqP*, *ctaA*, *narG*, *skfA*, *comGA*,
496 *aprE*, *cggR*, *spoIIIGA*, *spoVC*, and *tapA*, or to a region in the 3' part of *capE*, were amplified by
497 PCR from genomic DNA using appropriate pairs of primers (Supplementary Table S1). These
498 fragments were inserted by ligation-independent cloning in pBSB2 or in pBSB8, a pBSB2
499 derivative with the *gfpmut3* and *spec* (spectinomycin resistance) genes replaced by *mCherry*
500 (codon-optimised for *B. subtilis*) and *cm* (chloramphenicol resistance), respectively. The
501 resulting plasmids were then used to integrate each corresponding transcriptional fusion into
502 the chromosome of *B. subtilis* through single recombination. Transformation of *B. subtilis* was
503 performed according to standard procedures and the transformants were selected on Luria-
504 Bertani (LB, Sigma, France) plates supplemented with appropriate antibiotics at the following
505 concentrations: spectinomycin, 100µg/mL; chloramphenicol, 5µg/mL. Before each
506 experiment, cells were cultured on Tryptone Soya Agar (TSA, BioMérieux, France). Bacteria
507 were then grown in synthetic B-medium composed of (all final concentrations) 15mM
508 (NH₄)₂SO₄, 8mM MgSO₄·7H₂O, 27mM KCl, 7mM sodium citrate·2H₂O, 50mM Tris/HCl (pH
509 7.5), and 2mM CaCl₂·2H₂O, 1µM FeSO₄·7H₂O, 10µM MnSO₄·4H₂O, 0.6mM KH₂PO₄, 4.5mM
510 glutamic acid (pH 8), 862µM lysine, 784µM tryptophan, 1mM threonine and 0.5% glucose
511 were added before use⁶¹. Cultures for planktonic inoculum were prepared in 10mL B-medium
512 inoculated with a single colony and shaken overnight at 37°C. The culture was then diluted to

513 an OD_{600nm} of approximately 0.1 and grown at 37°C until it reached an OD_{600nm} of
 514 approximately 0.2. The procedure was repeated twice and finally the culture was grown to
 515 reach stationary phase, which was then used to inoculate swarming and liquid biofilm assays
 516 (Fig. 1).

517 **Table 1. *B. subtilis* strains used in this study**

Strain	Relevant genotype or isolation source	Construction or Reference ^a
NDmed	Undomesticated, isolated from endoscope washer-disinfectors	¹⁴
NDmed-GFP GM3649	NDmed <i>amyE::Phyperspank-gfpmut2</i> (spec)	¹⁵
BSB168	<i>trp+</i> derivative of 168	62,63
BBA093	BSB168 <i>PackA-gfpmut3</i> (spec)	M. Jules
BBA0231	BSB168 <i>Phag-gfpmut3</i> (spec)	M. Jules
BBA0290	BSB168 <i>PbslA-gfpmut3</i> (spec)	M. Jules
BBA0428	BSB168 <i>PsrfaA-gfpmut3</i> (spec)	M. Jules
BBA9006	BSB168 <i>PgapB-gfpmut3</i> (spec)	M. Jules
GM3346	NDmed <i>Phag-gfpmut3</i> (spec)	BBA0231→NDmed
GM3348	NDmed <i>PackA-gfpmut3</i> (spec)	BBA0093→NDmed
GM3378	NDmed <i>PgapB-gfpmut3</i> (spec)	BBA9006→NDmed
GM3401	NDmed <i>PbslA-gfpmut3</i> (spec)	BBA0290→NDmed
GM3402	BSB168 <i>PepsA-gfpmut3</i> (spec)	pBSB2epsA→BSB168
GM3403	NDmed <i>PsrfaA-gfpmut3</i> (spec)	BBA0428 →NDmed

GM3423	NDmed <i>PepsA-gfpmut3</i> (spec)	GM3402→NDmed
GM3461	BSB168 <i>PypqP-gfpmut3</i> (spec)	pBSB2ypqP→BSB168
GM3476	NDmed <i>PypqP-gfpmut3</i> (spec)	GM3461→NDmed
GM3816	NDmed <i>PctaA-gfpmut3</i> (spec)	pBSB2ctaA→NDmed
GM3820	NDmed <i>PnarG-mCherry</i> (cm)	pBSB8narG→NDmed
GM3823	NDmed <i>PskfA-mCherry</i> (cm)	pBSB8skfA→NDmed
GM3838	NDmed <i>PcomGA-gfpmut3</i> (spec)	pBSB2comGA→NDmed
GM3841	NDmed <i>PaprE-mCherry</i> (cm)	pBSB8aprE→NDmed
GM3859	NDmed <i>PcggR-mCherry</i> (cm)	pBSB8cggR→NDmed
GM3862	NDmed <i>capE-mCherry</i> (cm)	pBSB8capE→NDmed
GM3864	NDmed <i>PspoIIIGA-mCherry</i> (cm)	pBSB8spoIIIGA→NDmed
GM3867	NDmed <i>PspoVC-mCherry</i> (cm)	pBSB8spoVC→NDmed
GM3874	NDmed <i>PtapA-mCherry</i> (cm)	pBSB8tapA→NDmed
GM3900	NDmed <i>PgapB-gfpmut3</i> (spec)/ <i>PcggR-mCherry</i> (cm)	GM3859→GM3378
GM3903	NDmed <i>PaprE-mCherry</i> (cm)/ <i>PackA-gfpmut3</i> (spec)	GM3841→GM3348
GM3907	NDmed <i>PnarG-mCherry</i> (cm)/ <i>PctaA-gfpmut3</i> (spec)	GM3820→GM3816
GM3912	NDmed <i>PskfA-mCherry</i> (cm)/ <i>PcomGA-gfpmut3</i> (spec)	GM3838→GM3823
GM3924	NDmed <i>PtapA-mCherry</i> (cm)/ <i>Phag-gfpmut3</i> (spec)	GM3346→GM3874

518 ^a Arrows indicate transformation of pointed strain with indicated plasmid or chromosomal DNA of indicated
519 strain.

520 *Swarming culturing condition*

521 The OD₆₀₀ was measured and the culture was diluted, and 2µL of diluted bacterial culture
522 (adjusted to an OD_{600nm} of 0.01, ~10⁴ CFU) were inoculated at the centre of B-medium agar
523 plate and incubated for 24 hours at 30°C with 50% relative humidity. Plates (9cm diameter,
524 Greiner bio-one, Austria) containing 25mL agar medium (0.7% agar) were prepared 1 hour
525 before inoculation and dried with lids open for 5 minutes before inoculation.

526 *Liquid biofilm culturing condition*

527 Cultures were performed in microplates, either 3mL in 12-well microplate (Greiner bio-one,
528 Germany) or 150µL in 96-well microscopic grade microplate (µclear, Greiner bio-one,
529 Germany), inoculated from a stationary phase culture and adjusted to an OD_{600nm} of 0.01. The
530 plates were incubated at 30°C for 24 hours, followed by either local cell harvesting or
531 microscopic imaging. The 96-well plate was used for kinetic monitoring of the submerged
532 biofilm, and the pellicle was collected from a 12-well plate for observations. When necessary,
533 the medium was supplemented with 200µM isopropyl-β-d-thiogalactopyranoside (IPTG) to
534 induce Gfp expression from the *Phyperspank* promoter.

535 *Local mesoscopic cell harvest for RNA-seq*

536 For EX and ST phases (OD₆₀₀ ~0.6 and ~2.8, respectively), 6mL of each culture were collected and
537 pelleted by centrifugation at 8,000 × g at 4°C for 30 seconds. The pellet was then homogenised
538 by 500µl TRIzol reagent (Invitrogen, Carlsbad, CA, USA) for stabilising the RNA in the cell.
539 For the swarming model, using 24hr plates, four spatially localised compartments (MC, BS, DT
540 and TP) were collected independently. Collection was done manually by using a scraper
541 (SARSTEDT, USA) starting from the tips down to reach the mother colony (that was collected
542 by a loop). Cells of each localised compartment were collected from 16 plates in an Eppendorf
543 tube (CLEARline microtubes, Italy) containing 500µL TRIzol reagent. For a 24hr static liquid
544 model, 6 wells (from a 12-well microplate) were used to collect each sample. By using a scraper,
545 PL were collected in 6mL water. For DC, 1ml from the supernatant was collected from 6 wells.
546 For the SB collection, after discarding all the rest of the liquid, 1ml water was added in a well
547 and cells were collected by scratching with a pipet tip. Samples were centrifuged rapidly for 30
548 seconds (8,000 × g at 4°C) and pellets resuspended in 500µL Trizol.

549 A centrifugation step for all the above collections for 1 minute to discard the TRIzol reagent was
550 done and samples were snap-frozen by liquid nitrogen to be transferred to -80°C ready for the
551 RNA extraction step. For each of the 9 samples, 3 biological replicates were done.

552 *RNA extraction for RNA-seq*

553 For all nine different conditions, a washing step for the pellets of the *B. subtilis* NDmed was
554 done with 1mL TE (10mM Tris, 1mM EDTA, pH=8) + 60µl 1 M EDTA followed by
555 centrifugation for 30 seconds (8,000 × *g* at 4°C). Cell pellets were suspended in 1mL TRIzol
556 reagent. Cell suspension was transferred to a Fastprep screw cap tube containing 0.4g of glass
557 beads (0.1mm). Cells were disrupted by bead beating for 40 seconds at 6.5m/s in a FastPrep-
558 24 instrument (MP Biomedicals, United states). The supernatant was transferred to an
559 Eppendorf tube and chloroform (Sigma-Aldrich, France) was added in a ratio of 1:5, followed
560 by centrifugation at 8,000 × *g* for 15 minutes at 4°C. The chloroform step was repeated twice.
561 The aqueous phase was transferred to new Eppendorf, where sodium acetate (pH=5.8) was
562 added to a final concentration of 0.3M and 500µl of isopropanol (Sigma-Aldrich, France).
563 Samples were left overnight at -20°C and then centrifuged for 20 minutes. Pellets were washed
564 twice by 75% of ethanol (VWR, France) followed by centrifugation for 15 minutes at 4°C.
565 Then pellets were dried for 5 minutes under the hood. A RNA cleanup kit (Monarch RNA
566 Cleanup Kit T2050, New England Biolabs, France) was used to further clean the RNA samples.
567 Extracted RNA samples were stored in water RNAase/DNAse free (Ambion, United Kingdom)
568 at -80°C. Nanodrop and Bioanalyzer instruments were used for quantity and quality controls.
569 Library preparation including ribosomal RNA depletion and sequencing was performed by the
570 I2BC platform (Gif-sur-Yvette, France) using TruSeq Total RNA Stranded and Ribo-Zero
571 Bacteria Illumina kits, an Illumina NextSeq 550 system and NextSeq 500/550 High Output Kit
572 v2 to generate stranded single end reads (1 x 75bp).

573 *RNA-seq data analysis*

574 Primary data processing was performed by I2BC platform and consisted of: demultiplexing
575 (with bcl2fastq2-2.18.12), adapter trimming (Cutadapt 1.15), quality control (FastQC v0.11.5),
576 mapping (BWA v0.6.2-r126, ⁶⁴) against NDmed genome sequence (NCBI WGS project
577 accession JPVW01000000, ¹⁶). This generated between 13M and 29M of uniquely mapped
578 reads per sample which were summarised as read counts for 4028 genes (featureCounts, ⁶⁵)
579 after discarding 7 loci whose sequences also matched External RNA Controls Consortium

580 (ERCC) references. The downstream analysis was performed using R programming language.
581 Samples were compared by computing pairwise Spearman correlation coefficients (ρ) and
582 distance ($1-\rho$) on raw read counts which were summarised by a hierarchical clustering tree
583 (average-link). Detection of DEGs used R package “DESeq2” (v1.30.1, ⁶⁶) to estimate p-values
584 and \log_2 fold-changes. To control the false discovery rate, for each pair of conditions
585 compared, the vector of p-values served to estimate q-values with R package “fdrtool” (v1.2.16,
586 ⁶⁷). DEGs reported for pairwise comparisons of *B. subtilis* spatial compartments were based on
587 a $q\text{-value} \leq 0.05$ and, unless stated otherwise, $|\log_2\text{FC}| \geq 1$. Fragment counts normalised per
588 kilobase of feature length per million mapped fragments (fpkm) computed by DESeq2 based
589 on robust estimation of library size were used as values of expression levels for each gene in
590 each sample. Genes were compared for their expression profiles across samples for selected
591 sets of conditions based on pairwise Pearson correlation coefficients (r) and distance ($1-r$)
592 computed on $\log_2(\text{fpkm}+5)$ and average-link hierarchical clustering of the distance matrix.
593 Accordingly, the associated heatmaps represent gene-centred variations of $\log_2(\text{fpkm}+5)$
594 values across samples. Gene clusters defined by cutting the hierarchical clustering trees at
595 height 0.3 (corresponding to average r within group of 0.7) were numbered by decreasing
596 number of the genes coupled in the same group, G1 for the largest. The resulting gene clusters
597 were systematically compared to *Subtiwiki* functional categories and regulons³⁸ (from
598 hierarchical level 1 to level 5) using exact Fisher test applied to 2×2 matrices. The results of
599 the comparisons with *Subtiwiki* functional categories were summarised in the form of stacked
600 bar plots after manually assigning each gene to the most relevant category in the context of this
601 study (when the same gene belonged to several categories) and a grouping of categories
602 corresponding to hierarchical level 2 excepted for “Metabolism” (level 1), and “motility and
603 chemotaxis” and “biofilm formation” (level 3). The whole transcriptomic data set has been
604 deposited in GEO (accession number [GSE214964](#)).

605 *CLSM*

606 The biofilm models were observed using a Leica SP8 AOBS inverted laser scanning
607 microscope (CLSM, LEICA Microsystems, Wetzlar, Germany) at the INRAE MIMA2
608 platform (<https://doi.org/10.15454/1.5572348210007727E12>). For observation, strains were
609 tagged fluorescently in green with SYTO 9 (0.5:1000 dilution in water from a stock solution at
610 $5\mu\text{M}$ in DMSO; Invitrogen, France) and SYTO 61 (1:1000 dilution in water from a stock
611 solution at $5\mu\text{M}$ in DMSO; Invitrogen, France), a nucleic acid marker. After 15 to 20 minutes

612 of incubation in the dark at 30 °C to enable fluorescent labelling of the bacteria, plates were
613 then mounted on the motorised stage of the confocal microscope. For the carbon metabolism
614 reporting genes, the 3D (xyz) acquisitions were performed by a HC PL FLUOTAR 10x /0.3
615 DRY objective (512 × 512 pixels, pixel size 0.361 μm, 1 image every z = 20 μm with a scan
616 speed of 600 Hz, and a pinhole70μm) to be able to capture the submerged and the pellicle in
617 the same well. Moreover, the different selected compartments were scanned using either HC
618 PL APO CS2 63x/1.2 water immersion or 10x objective lenses. SYTO 9, Gfp and IP excitation
619 was performed at 488 nm with an argon laser, and the emitted fluorescence was recorded within
620 the ranges 500-550 nm and 600–750 nm, respectively on hybrid detectors. SYTO 61 or
621 mCherry excitation was performed at 561 nm with an argon laser, and the emitted fluorescence
622 was recorded within the range 600–750 nm on hybrid detectors. The 3D (xyz) acquisitions
623 were performed (512 × 512 pixels, pixel size 0.361 μm, 1 image every z = 1 μm with a scan
624 speed of 600 Hz). For 4D (xyzt) acquisitions an image was taken every 1 hour for 48 hours or
625 1 and half hours for 72 h.

626 The whole 4D-CLM data set has been deposited in Recherche Data Gouv
627 (<https://doi.org/10.57745/Z511A6>).

628 *Image analysis*

629 Projections of the biofilm, 3D or 4D were constructed from Z-series images using IMARIS 9.3
630 (Bitplane, Switzerland). Space-time kymographs were constructed with the BiofilmQ
631 visualisation toolbox from 4D-CLSM series⁶⁸.

632

633 **ACKNOWLEDGEMENTS**

634 This work was supported by INRAE. Y. Dergham is the recipient of fundings from the Union
635 of Southern Suburbs Municipalities of Beirut, INRAE, Campus France PHC CEDRE 42280PF
636 and Fondation AgroParisTech. P. Sanchez-Vizuete was the recipient of a PhD grant from the
637 Région Ile-de-France (DIM ASTREA). Pr. M. Jules (University Paris-Saclay, AgroParisTech,
638 INRAE) is acknowledged for the gift of plasmids pBSB2 and pBSB8, and of strains BBA0093,
639 BBA0231, BBA0290, BBA0428 and BBA9006. M. Calabre (INRAE) is acknowledged for
640 technical assistance. We acknowledge the sequencing and bioinformatics expertise of the I2BC
641 High-throughput sequencing facility, supported by France Génomique (funded by the French

642 National Program “Investissement d’Avenir” ANR-10-INBS-09). Biofilm imaging was
643 realized at the INRAE MIMA2 imaging platform
644 <https://doi.org/10.15454/1.5572348210007727E12>. This work is performed under the umbrella
645 of the European Space Agency Topical Team: Biofilms from an interdisciplinary perspective.

646 **Author contributions**

647 Y.D., D.L.C, K.H. and R.B. designed research; Y.D., D.L.C, E.H., J.D. and P.S.V performed
648 research; Y.D., P.N., D.L.C and R.B analysed data; Y.D., D.L.C, P.N., K.H. and R.B. wrote
649 the manuscript with support from all authors.

650

651 **References**

- 652 1. Vlamakis H, Chai Y, Beaugard P, Losick R, Kolter R. Sticking together:
653 Building a biofilm the *Bacillus subtilis* way. *Nat Rev Microbiol.* 2013;11(3):157-
654 168. doi:10.1038/nrmicro2960
- 655 2. Flemming HC, Wingender J, Szewzyk U, Steinberg P, Rice SA, Kjelleberg S.
656 Biofilms: an emergent form of bacterial life. *Nat Rev Microbiol.* 2016 Aug
657 11;14(9):563-75. doi: 10.1038/nrmicro.2016.94. PMID: 27510863
- 658 3. Stewart PS, Franklin MJ. Physiological heterogeneity in biofilms. *Nat Rev*
659 *Microbiol.* 2008;6(3):199-210. doi:10.1038/nrmicro1838
- 660 4. Lemon KP, Earl AM, Vlamakis HC, Aguilar C, Kolter R. Biofilm Development
661 with an Emphasis on *Bacillus subtilis*. *Curr Top Microbiol Immunol.*
662 2008;322(1):1-16. doi:10.1007/978-3-540-75418-3
- 663 5. Bridier A, Le Coq D, Dubois-Brissonnet F, Thomas V, Stéphane A, Briandet R.
664 The Spatial Architecture of *Bacillus subtilis* Biofilms Deciphered Using a
665 Surface-Associated Model and In Situ Imaging. *PLoS One.* 2011;6(1):e16177.
666 doi:10.1371/journal.pone.0016177
- 667 6. Branda SS, González-Pastor JE, Ben-Yehuda S, Losick R, Kolter R. Fruiting
668 Body Formation by *Bacillus Subtilis*. *Proc Natl Acad Sci USA.*
669 2001;25;98(20):11621-6. doi: 10.1073/pnas.191384198
- 670 7. Dergham Y, Sanchez-Vizuite P, Le Coq D, et al. Comparison of the Genetic
671 Features Involved in *Bacillus subtilis* Biofilm Formation Using Multi-Culturing
672 Approaches. *Microorganisms.* 2021;9(633).
673 doi:10.3390/microorganisms9030633

- 674 8. Barbosa TM, Serra CR, Ragione RM La, Woodward MJ, Henriques AO.
675 Screening for *Bacillus* Isolates in the Broiler Gastrointestinal Tract. *Appl Environ*
676 *Microbiol.* 2005;71(2):968-978. doi:10.1128/AEM.71.2.968-978.2005
- 677 9. Hong HA, Khaneja R, Tam NMK, et al. *Bacillus subtilis* isolated from the human
678 gastrointestinal tract. *Res Microbiol.* 2009;160(2):134-143.
679 doi:10.1016/j.resmic.2008.11.002
- 680 10. Bais HP, Fall R, Vivanco JM. Biocontrol of *Bacillus subtilis* against Infection of
681 *Arabidopsis* Roots by *Pseudomonas syringae* Is Facilitated by Biofilm Formation
682 and Surfactin Production. *Plant Physiol.* 2004;134:307-319.
683 doi:10.1104/pp.103.028712
- 684 11. Marzorati M, Van den Abbeele P, Bubeck SS, et al. *Bacillus subtilis* HU58 and
685 *Bacillus coagulans* SC208 probiotics reduced the effects of antibiotic-induced gut
686 microbiome dysbiosis in an M-SHIME® model. *Microorganisms.* 2020;8(7):1-
687 15. doi:10.3390/microorganisms8071028
- 688 12. Lefevre M, Racedo SM, Denayrolles M, et al. Safety assessment of *Bacillus*
689 *subtilis* CU1 for use as a probiotic in humans. *Regul Toxicol Pharmacol.*
690 2017;83:54-65. doi:10.1016/j.yrtph.2016.11.010
- 691 13. Guéneau V, Plateau-Gonthier J, Arnaud L, Piard JC, Castex M, Briandet R.
692 Positive biofilms to guide surface microbial ecology in livestock buildings.
693 *Biofilm.* 2022;4. doi:10.1016/j.bioflm.2022.100075
- 694 14. Martin DJH, Denyer SP, McDonnell G, Maillard JY. Resistance and cross-
695 resistance to oxidising agents of bacterial isolates from endoscope washer
696 disinfectors. *J Hosp Infect.* 2008;69(4):377-383. doi:10.1016/j.jhin.2008.04.010
- 697 15. Bridier A, de Sanchez-Vizuete MP, Le Coq D, et al. Biofilms of a *Bacillus subtilis*
698 Hospital Isolate Protect *Staphylococcus aureus* from Biocide Action. *PLoS One.*
699 2012;7(9). doi:10.1371/journal.pone.0044506
- 700 16. Sanchez-Vizuete P, Tanaka K, Bridier A, et al. Genome Sequences of Two
701 Nondomesticated *Bacillus subtilis* Strains Able To Form Thick Biofilms on
702 Submerged Surfaces. *Genome Announc.* 2014;25(2):5.
703 doi:10.1128/genomeA.00946-14
- 704 17. Klein W, Weber MHW, Marahiel MA. Cold shock response of *Bacillus subtilis*:
705 Isoleucine-dependent switch in the fatty acid branching pattern for membrane
706 adaptation to low temperatures. *J Bacteriol.* 1999;181(17):5341-5349.
707 doi:10.1128/jb.181.17.5341-5349.1999

- 708 18. Hoffmann T, Bremer E. Protection of *Bacillus subtilis* against cold stress via
709 compatible-solute acquisition. *J Bacteriol.* 2011;193(7):1552-1562.
710 doi:10.1128/JB.01319-10
- 711 19. Lopez D, Vlamakis H, Kolter R. Generation of multiple cell types in *Bacillus*
712 *subtilis*. *FEMS Microbiol Rev.* 2009;33(1):152-163. doi:10.1111/j.1574-
713 6976.2008.00148.x
- 714 20. Hamon MA, Lazazzera BA. The sporulation transcription factor Spo0A is
715 required for biofilm development in *Bacillus subtilis*. *Mol Microbiol.*
716 2001;42(5):1199-1209. doi:10.1046/j.1365-2958.2001.02709.x
- 717 21. Harshey RM. Bacterial motility on a surface: many ways to a common goal. *Annu*
718 *Rev Microbiol.* 2003;57:249-273. doi:10.1146/annurev.micro.57.030502.091014
- 719 22. Julkowska D, Obuchowski M, Holland IB, Séror SJ. Branched swarming patterns
720 on a synthetic medium formed by wild-type *Bacillus subtilis* strain 3610:
721 Detection of different cellular morphologies and constellations of cells as the
722 complex architecture develops. *Microbiology.* 2004;150(6):1839-1849.
723 doi:10.1099/mic.0.27061-0
- 724 23. Julkowska D, Obuchowski M, Holland IB, Séror SJ. Comparative analysis of the
725 development of swarming communities of *Bacillus subtilis* 168 and a natural wild
726 type: Critical effects of surfactin and the composition of the medium. *J Bacteriol.*
727 2005;187(1):65-76. doi:10.1128/JB.187.1.65-76.2005
- 728 24. Hamze K, Julkowska D, Autret S, et al. Identification of genes required for
729 different stages of dendritic swarming in *Bacillus subtilis*, with a novel role for
730 *phrC*. *Microbiology.* 2009;155(2):398-412. doi:10.1099/mic.0.021477-0
- 731 25. Hamouche L, Laalami S, Daerr A, et al. *Bacillus subtilis* Swarmer Cells Lead the
732 Swarm, Multiply, and Generate a Trail of Quiescent Descendants. *MBio.*
733 2017;8(1):1-14. doi:https://doi.org/10.1128/mBio.02102-16.
- 734 26. Grobas I, Polin M, Asally M. Swarming bacteria undergo localized dynamic
735 phase transition to form stress-induced biofilms. *Elife.* 2021;10:1-22.
736 doi:10.7554/eLife.62632
- 737 27. Sanchez-Vizuite P, Le Coq D, Bridier A, Herry J-M, Aymerich S, Briandet R.
738 Identification of *ypqP* as a New *Bacillus subtilis* Biofilm Determinant That
739 Mediates the Protection of *Staphylococcus aureus* against Antimicrobial Agents
740 in Mixed-Species Communities. *Appl Env Microbiol.* 2015;81(1):109-118.
741 doi:10.1128/AEM.02473-14

- 742 28. Vlamakis H, Aguilar C, Losick R, Kolter R. Control of cell fate by the formation
743 of an architecturally complex bacterial community. *Genes Dev.* 2008;22(7):945-
744 953. doi:<https://doi.org/10.1101/gad.1645008>
- 745 29. López D, Kolter R. Extracellular signals that define distinct and coexisting cell
746 fates in *Bacillus subtilis*. *FEMS Microbiol Rev.* 2010;34(2):134-149.
747 doi:10.1111/j.1574-6976.2009.00199.x
- 748 30. Kearns DB, Losick R. Cell population heterogeneity during growth of *Bacillus*
749 *subtilis*. *Genes Dev.* 2005;19(24):3083-3094. doi:10.1101/gad.1373905
- 750 31. Nakano MM, Magnuson R, Myers A, Curry J, Grossman AD, Zuber P. *urfA* is an
751 operon required for surfactin production, competence development, and efficient
752 sporulation in *Bacillus subtilis*. *J Bacteriol.* 1991;173(5):1770-1778.
753 doi:10.1128/jb.173.5.1770-1778.1991
- 754 32. Ostrowski A, Mehert A, Prescott A, Kiley TB, Stanley-Wall NR. YuaB Functions
755 Synergistically with the Exopolysaccharide and TasA Amyloid Fibers To Allow
756 Biofilm Formation by *Bacillus subtilis*. *J Bacteriol.* 2011;193(18):4821-4831.
757 doi:10.1128/JB.00223-11
- 758 33. Hobley L, Ostrowski A, Rao F V., et al. BslA is a self-assembling bacterial
759 hydrophobin that coats the *Bacillus subtilis* biofilm. *PNAS.* 2013;98(20):11621-
760 11626. doi:10.1073/pnas.191384198
- 761 34. van Gestel J, Vlamakis H, Kolter R. From Cell Differentiation to Cell Collectives:
762 *Bacillus subtilis* Uses Division of Labor to Migrate. *PLoS Biol.* 2015;13(4):1-29.
763 doi:10.1371/journal.pbio.1002141
- 764 35. Pisithkul T, Schroeder JW, Trujillo EA, et al. Metabolic Remodeling during
765 Biofilm Development of *Bacillus subtilis*. *MBio.* 2019;10(3).
766 doi:10.1128/mBio.00623-19
- 767 36. Futo M, Opa Si L, Koska S, et al. Embryo-Like Features in Developing *Bacillus*
768 *subtilis* Biofilms. *Mol Biol Evol.* 2020;38(1):31-47.
769 doi:10.1093/molbev/msaa217
- 770 37. Sanchez-Vizuete P, Dergham Y, Bridier A, et al. The coordinated population
771 redistribution between *Bacillus subtilis* submerged biofilm and liquid-air pellicle.
772 *Biofilm.* 2021. doi.org/10.1016/j.bioflm.2021.100065
- 773 38. Zhu B, Stülke J. SubtiWiki in 2018: From genes and proteins to functional
774 network annotation of the model organism *Bacillus subtilis*. *Nucleic Acids Res.*
775 2018;46(D1):D743-D748. doi:10.1093/nar/gkx908

- 776 39. Paul S, Zhang X, Hulett FM. Two ResD-controlled promoters regulate *ctaA*
777 expression in *Bacillus subtilis*. *J Bacteriol.* 2001;183(10):3237-3246.
778 doi:10.1128/JB.183.10.3237-3246.2001
- 779 40. Fillinger S, Boschi-Muller S, Azza S, Dervyn E, Branlant G, Aymerich S. Two
780 glyceraldehyde-3-phosphate dehydrogenases with opposite physiological roles in
781 a nonphotosynthetic bacterium. *J Biol Chem.* 2000;275(19):14031-14037.
782 doi:10.1074/jbc.275.19.14031
- 783 41. Tännler S, Fischer E, Le Coq D, et al. CcpN controls central carbon fluxes in
784 *Bacillus subtilis*. *J Bacteriol.* 2008;190(18):6178-6187. doi:10.1128/JB.00552-
785 08
- 786 42. Ludwig H, Homuth G, Schmalisch M, Dyka FM, Hecker M, Stülke J.
787 Transcription of glycolytic genes and operons in *Bacillus subtilis*: Evidence for
788 the presence of multiple levels of control of the *gapA* operon. *Mol Microbiol.*
789 2001;41(2):409-422. doi:10.1046/j.1365-2958.2001.02523.x
- 790 43. Servant P, Le Coq D, Aymerich S. CcpN (YqzB), a novel regulator for CcpA-
791 independent catabolite repression of *Bacillus subtilis* gluconeogenic genes. *Mol*
792 *Microbiol.* 2005;55(5):1435-1451. doi:10.1111/j.1365-2958.2005.04473.x
- 793 44. Houry A, Gohar M, Deschamps J, et al. Bacterial swimmers that infiltrate and
794 take over the biofilm matrix. *PNAS.* 2012;109(32). doi:10.1073/pnas.1200791109
- 795 45. Dubois T, Krzewinski F, Yamakawa N, et al. The *sps* genes encode an original
796 legionaminic acid pathway required for crust assembly in *Bacillus subtilis*. *MBio.*
797 2020;11(4):1-17. doi:10.1128/mBio.01153-20
- 798 46. Guilhen C, Miquel S, Charbonnel N, et al. Colonization and immune modulation
799 properties of *Klebsiella pneumoniae* biofilm-dispersed cells. *npj Biofilms*
800 *Microbiomes.* 2019;5(1). doi:10.1038/s41522-019-0098-1
- 801 47. Guilhen C, Charbonnel N, Parisot N, et al. Transcriptional profiling of *Klebsiella*
802 *pneumoniae* defines signatures for planktonic, sessile and biofilm-dispersed cells.
803 *BMC Genomics.* 2016;17(1). doi:10.1186/s12864-016-2557-x
- 804 48. Chua SL, Liu Y, Yam JKH, et al. Dispersed cells represent a distinct stage in the
805 transition from bacterial biofilm to planktonic lifestyles. *Nat Commun.* 2014;5.
806 doi:10.1038/ncomms5462
- 807 49. Pettigrew MM, Marks LR, Kong Y, Gent JF, Roche-Hakansson H, Hakansson
808 AP. Dynamic changes in the *Streptococcus pneumoniae* transcriptome during
809 transition from biofilm formation to invasive disease upon influenza A virus
810 infection. *Infect Immun.* 2014;82(11):4607-4619. doi:10.1128/IAI.02225-14

- 811 50. Arnaouteli S, Ferreira AS, Schor M, et al. Bifunctionality of a biofilm matrix
812 protein controlled by redox state. *Proc Natl Acad Sci U S A*. 2017;114(30):E6184-
813 E6191. doi:10.1073/pnas.1707687114
- 814 51. Zeriouh H, de Vicente A, Pérez-García A, Romero D. Surfactin triggers biofilm
815 formation of *Bacillus subtilis* in melon phylloplane and contributes to the
816 biocontrol activity. *Environ Microbiol*. 2014;16(7):2196-2211.
817 doi:10.1111/1462-2920.12271
- 818 52. Chen XH, Koumoutsi A, Scholz R, et al. Genome analysis of *Bacillus*
819 *amyloliquefaciens* FZB42 reveals its potential for biocontrol of plant pathogens.
820 *J Biotechnol*. 2009;140(1-2):27-37. doi:10.1016/j.jbiotec.2008.10.011
- 821 53. Thérien M, Kiesewalter HT, Auria E, et al. Surfactin production is not essential
822 for pellicle and root-associated biofilm development of *Bacillus subtilis*. *Biofilm*.
823 2020;2:100021. doi:10.1016/J.BIOFLM.2020.100021
- 824 54. Shivers RP, Dineen SS, Sonenshein AL. Positive regulation of *Bacillus subtilis*
825 *ackA* by CodY and CcpA: Establishing a potential hierarchy in carbon flow. *Mol*
826 *Microbiol*. 2006;62(3):811-822. doi:10.1111/j.1365-2958.2006.05410.x
- 827 55. López D, Fischbach MA, Chu F, Losick R, Kolter R. Structurally diverse natural
828 products that cause potassium leakage trigger multicellularity in *Bacillus subtilis*.
829 *Proc Natl Acad Sci U S A*. 2009;106(1):280-285. doi:10.1073/pnas.0810940106
- 830 56. D'Souza C, Nakano MM, Zuber P. Identification of *comS*, a gene of the *srfA*
831 operon that regulates the establishment of genetic competence in *Bacillus subtilis*.
832 *Proc Natl Acad Sci U S A*. 1994;91(20):9397-9401. doi:10.1073/pnas.91.20.9397
- 833 57. Asally M, Kittisopikul M, Rué P, et al. Localized cell death focuses mechanical
834 forces during 3D patterning in a biofilm. *Proc Natl Acad Sci U S A*.
835 2012;109(46):18891-18896. doi:10.1073/pnas.1212429109
- 836 58. Wilking JN, Zaburdaev V, De Volder M, Losick R, Brenner MP, Weitz DA.
837 Liquid transport facilitated by channels in *Bacillus subtilis* biofilms. *Proc Natl*
838 *Acad Sci U S A*. 2013;110(3):848-852. doi:10.1073/pnas.1216376110
- 839 59. Ellwood DC, Tempest DW. Control of teichoic acid and teichuronic acid
840 biosyntheses in chemostat cultures of *Bacillus subtilis* var. *niger*. *Biochem J*.
841 1969;111(1):1-5. doi:10.1042/bj1110001
- 842 60. Botella E, Fogg M, Jules M, et al. pBaSysBioII: An integrative plasmid
843 generating *gfp* transcriptional fusions for high-throughput analysis of gene
844 expression in *Bacillus subtilis*. *Microbiology*. 2010;156(6):1600-1608.
845 doi:10.1099/mic.0.035758-0

- 846 61. Antelmann H, Engelmann S, Schmid R, Sorokin A, Lapidus A, Hecker M.
847 Expression of a stress- and starvation-induced *dps/pexB*-homologous gene is
848 controlled by the alternative sigma factor $\sigma(B)$ in *Bacillus subtilis*. *J Bacteriol.*
849 1997;179(23):7251-7256. doi:10.1128/jb.179.23.7251-7256.1997
- 850 62. Nicolas P, Mäder U, Dervyn E, et al. Condition-dependent transcriptome reveals
851 high-level regulatory architecture in *Bacillus subtilis*. *Science (80-)*.
852 2012;335(March):1103-1106.
- 853 63. Buescher JM, Liebermeister W, Jules M, et al. Global network reorganization
854 during dynamic adaptations of *Bacillus subtilis* metabolism. *Science (80-)*.
855 2012;335(6072):1099-1103. doi:10.1126/science.1206871
- 856 64. Li H, Durbin R. Fast and accurate short read alignment with Burrows-Wheeler
857 transform. *Bioinformatics.* 2009;25(14):1754-1760.
858 doi:10.1093/bioinformatics/btp324
- 859 65. Liao Y, Smyth GK, Shi W. FeatureCounts: An efficient general purpose program
860 for assigning sequence reads to genomic features. *Bioinformatics.*
861 2014;30(7):923-930. doi:10.1093/bioinformatics/btt656
- 862 66. Love MI, Huber W, Anders S. Moderated estimation of fold change and
863 dispersion for RNA-seq data with DESeq2. *Genome Biol.* 2014;15(12):1-21.
864 doi:10.1186/s13059-014-0550-8
- 865 67. Strimmer K. A unified approach to false discovery rate estimation. *BMC*
866 *Bioinformatics.* 2008;9. doi:10.1186/1471-2105-9-303
- 867 68. Hartmann R, Jeckel H, Jelli E, et al. Quantitative image analysis of microbial
868 communities with BiofilmQ. *Nat Microbiol.* 2021;6(2):151-156.
869 doi:10.1038/s41564-020-00817-4